GEOPHYSICAL RESEARCH LETTERS, VOL. 28, NO. 10, PAGES 2117-2120, MAY 15, 2001

Measurement of interseismic strain accumulation across the North Anatolian Fault by satellite radar interferometry

Tim Wright, Barry Parsons, and Eric Fielding[1]

Department of Earth Sciences, University of Oxford, Parks Road, Oxford, UK.

Abstract. In recent years, interseismic crustal velocities and strains have been determined for a number of tectonically active areas through repeated measurements using the Global Positioning System. The terrain in such areas is often remote and difficult, and the density of GPS measurements relatively sparse. In principle, satellite radar interferometry can be used to make millimetric-precision measurements of surface displacement over large surface areas. In practice, the small crustal deformation signal is dominated over short time intervals by errors due to atmospheric, topographic and orbital effects. Here we show that these effects can be overcome by stacking multiple interferograms, after screening for atmospheric anomalies, effectively creating a new interferogram that covers a longer time interval. In this way, we have isolated a 70 km wide region of crustal deformation across the eastern end of the North Anatolian Fault, Turkey. The distribution of deformation is consistent with slip of 17–32 mm/yr below 5–33 km on the extension of the surface fault at depth. If the GPS determined slip rate of 24±1 mm/yr is accepted, the locking depth is constrained to 18±6 km.

Introduction

The use of InSAR for the measurement of large ground movements associated with earthquakes is now a well established technique [*Massonnet et al.*, 1993; *Massonnet and Feigl*, 1998; *Bürgmann et al.*, 2000]. Fault creep has also been measured using interferometry, *e.g.*[*Rosen et al.*, 1998]; the ground displacements caused by creep are discontinuous, producing steps in interferograms that are relatively easy to detect. Interseismic crustal deformation, however, seldom exceeds rates of a few 10's of millimetres per year distributed over 30-150 km (strain rates of $3 \times 10^{-8} - 5 \times 10^{-7}$ yr^{-1}) and, to date, it has proved difficult to measure using radar interferometry. To overcome the limited coherence between SAR images over long intervals, and to enhance the crustal strain signal relative to atmospheric and orbital errors, we combined multiple interferograms [*Zebker et al.*, 1997], constructed from SAR images acquired by the ERS-1 and ERS-2 satellites. In this way we create an interferogram corresponding to a time interval longer than can be obtained directly.

[1]Also at Jet Propulsion Lab, Caltech, USA.

Paper number 2000GL012850.
0094-8276/01/2000GL012850$05.00

The North Anatolian Fault Zone (Fig. 1a) is one of the longest and most active strike-slip fault zones in the world [*Barka*, 1996]. In comparison to the analogous San Andreas Fault Zone in California, relatively little is known about the North Anatolian Fault Zone. In particular, few geodetic data exist along most of its length (east of 31°E) [*McClusky et al.*, 2000], and the distribution of interseismic strain there is unknown. It is a good target for InSAR because of its east-west orientation and the semi-arid climate in parts.

InSAR data

We analysed 12 interferometric pairs across the North Anatolian Fault with temporal separations between 1.2 and 3.8 years and altitudes of ambiguity (the magnitude of topographic error that will cause a 2π phase error) greater than 250 m (Fig. 2). A 40 m-resolution digital elevation model (DEM), constructed from ERS tandem pairs (Fig. 1a), was used to remove the topographic contribution to phase. The tandem DEM was calibrated by comparison to a 3-arcsecond (∼90 m) DEM from the US Department of Defence (believed to have elevation errors < 50 m). To minimise the topographic errors arising from variations in atmospheric water vapour, we constructed DEMs from 5 distinct tandem pairs, and used the one with the smallest residuals relative to the 90 m DEM. The rms residual height of this tandem DEM with respect to the existing DEM is 32 m: 0.7 radians of erroneous phase with the smallest altitude of ambiguity. In addition, the residual heights have short wavelengths (< 10 km), and would not give rise to the monotonic variations in phase expected across the fault. The signal-to-noise ratio of each interferogram was improved by averaging the phase, to create datasets with 160 m pixel spacing, and by using a weighted power spectrum filter [*Goldstein and Werner*, 1998].

Four of the interferograms contained no usable interferometric data because of a lack of coherence. Of the coherent interferograms, four contained areas of high phase gradient, often around topographic features. These are likely to be atmospheric artefacts, arising from changes in the path length due to different amounts of atmospheric water vapour in the two images, *e.g.*[*Delacourt et al.*, 1998]. The remaining four interferograms (Fig. 1b–e) have gentle gradients: the 1-σ variance of phase for any one interferogram is less than 3 radians. These were unwrapped interactively to remove the 2π phase ambiguity and summed to create an interferogram with an equivalent time span of 7.4 years (Fig. 1f).

The precise orbits from Delft University [*Scharroo and Visser*, 1998] used in constructing the interferograms have a radial precision of ∼7 cm. Uncertainties in the satellite po-

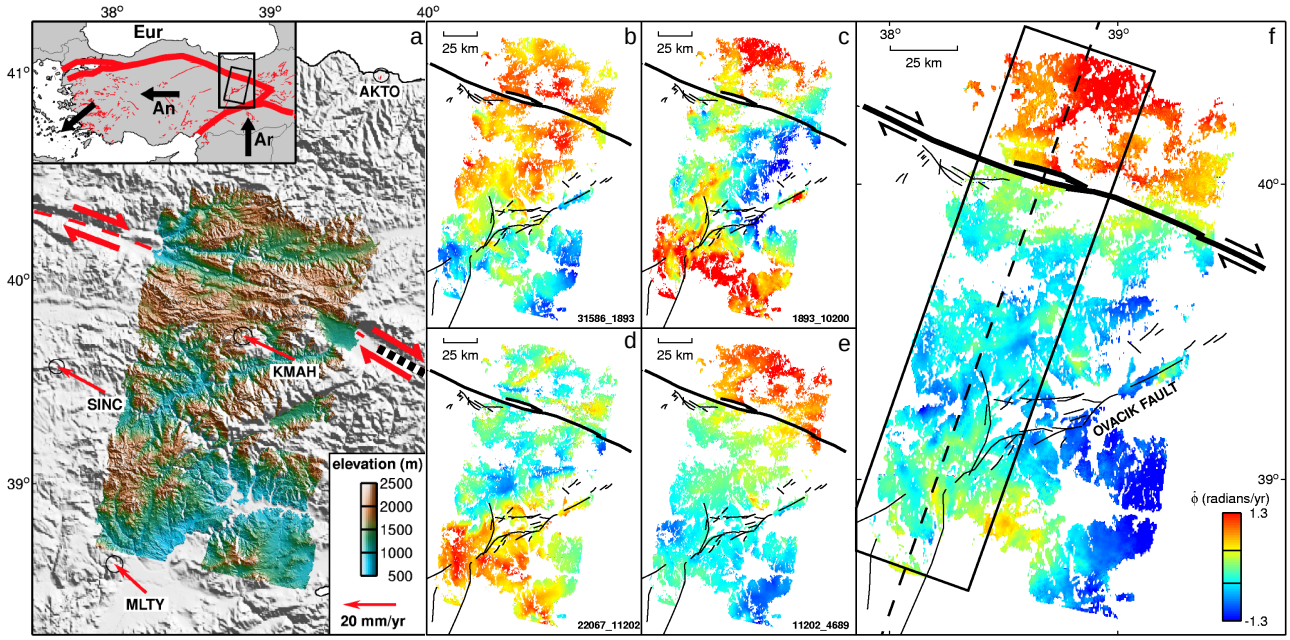

Figure 1. a, Map of the eastern end of the North Anatolian Fault. The colored area shows the 40m resolution DEM that we derived using ERS tandem images (track 35, frames 2801,2819, orbits 31586(ERS-1) and 11913(ERS-2)). Outside the coloured area, shaded relief from GTOPO30 is plotted. Arrows are GPS-determined velocities relative to Eurasia [*McClusky et al.*, 2000], and the North Anatolian Fault is marked as a dashed, red line with the location of the 1992 Erzincan earthquake shown as a dashed black line. The remainder of the fault in this area ruptured in the 1939 earthquake [*Barka*, 1996]. The inset illustrates schematic plate configurations (Eur=Eurasia,Ar=Arabia,An=Anatolia). **b–e**, Individual interseismic interferograms (orbit numbers shown), generated using the DIAPASON interferometric software (©CNES), unwrapped and scaled by the time interval so that each is an estimate of the yearly phase change ($\dot{\phi}$). **f**, Mean $\dot{\phi}$, calculated by summing the individual unwrapped interferograms and dividing by the total time interval (7.4 years). Positive $\dot{\phi}$ (warm colors) indicate a relative decrease in distance to the satellite. The rectangular box delimits data used to construct the phase profile (Fig. 3a). Black lines are mapped faults [*Şaroglu et al.*, 1992] with the North Anatolian Fault shown in bold.

sition are greater than those in the change in position over 200 km of the satellite track, resulting in larger orbital phase

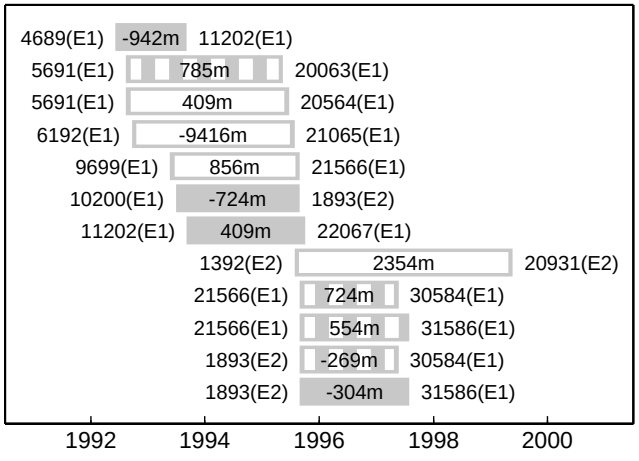

Figure 2. Interferometric data used. The ERS orbit numbers are shown on either side of a bar whose length represents the temporal separation of the images that form the interferogram. The scene-centre altitude of ambiguity is given at the centre of the bar. Only interferograms represented by solid bars were used in the determination of crustal strain: those represented by white bars were incoherent, strong atmospheric artefacts were exhibited in those with dashed bars. SAR data (©ESA) are from track 35, frames 2801/2819.

gradients perpendicular to the track than parallel to it. A linear gradient perpendicular to the track was removed from each interferogram to flatten the phase (Fig. 1b–e). A small erroneous phase gradient parallel to the track may still be present in each of the interferograms ($\leq$ 0.5 fringes/100 km). Because these tilts are similar to the signal expected from interseismic strain, we extended the four best interferograms for a further 100 km to the south where the deformation signal should be small. In the final stacked interferogram, we find that any small orbital errors have cancelled such that, farther than ∼50 km south of the fault, phase is approximately constant, and in good agreement with the few GPS measurements available.

The stacked interferogram (Fig. 1f) shows a strong phase change, of ∼15 radians, centred on the surface trace of the North Anatolian Fault but distributed over ∼70 km. There remains some variability (∼4 radians), correlated over spatial wavelengths of 20–50km, that probably arises from atmospheric heterogeneities. To further enhance the deformation signal, assuming that it varies slowly along the fault, we created an averaged profile covering a 50 km wide swath of the more complete western half of the stacked interferogram (Fig. 3a). Average phase values were calculated every 5 km in 10 km bins along the profile. Although each value on the profile averages over a large number of phase measurements (∼10–20,000), the spatial correlation of the atmospheric errors over distances larger than the bin size means that the formal uncertainties will underestimate the actual errors. The phase variation within each 10 by 50 km bin gives a

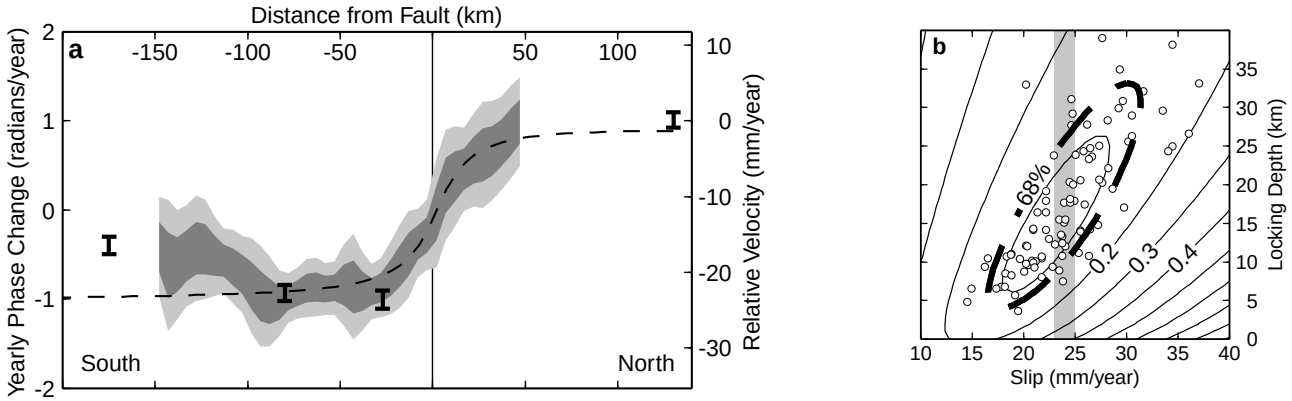

Figure 3. **a**, Phase profile perpendicular to the North Anatolian Fault. The thick grey bands delimit the 1- and 2-σ error bounds on phase, measured in the box shown in Fig. 1f. Black bars are the GPS velocities and error bounds [*McClusky et al.*, 2000] projected onto the profile and converted into phase change. The conversion from phase change to relative velocity assumes pure horizontal motion parallel to the North Anatolian Fault (vertical line). Velocities predicted by our best-fitting slip model (22 mm/yr under a 14 km elastic lid) are plotted as a dashed line. **b**, Solution-space plot for the fault model. Contours show the rms misfit (0.1 radians/yr interval) to the unperturbed phase profile. Circles are 100 best-fit parameters from a Monte-Carlo simulation of 100 perturbed profiles, each created by adding a different perturbation profile to the observed phase profile. (To account for correlated atmospheric errors, the perturbation profiles consisted of random phase values every L km, calculated using the standard error at that location, with linear ramps in between. Because atmospheric errors are correlated on a 20–50 km wavelength in these interferograms, a different value of L was chosen randomly from this range for each profile.) The errors of the model parameters are given by the distribution of solutions. The 68% confidence limit (dashed ellipse) is found to correspond to a 0.12 radians/year rms misfit to the observed phase values. The vertical grey bar corresponds to the slip rate determined from GPS.

more realistic estimate of error because it includes the long-wavelength, correlated phase signal from the atmosphere.

The section of the North Anatolian Fault covered by our interferometric data last ruptured during an earthquake in 1939 [*Barka*, 1996]. Hence, any post-seismic deformation is likely to be negligible, if current estimates of the time-scale for post-seismic relaxation, *e.g.*[*Scholz*, 1990], are correct. However, in 1992, a M_w=6.8 earthquake ruptured 30 km of the North Anatolian Fault at Erzincan, 100 km east of our phase profile (Fig. 1a; [*Barka and Eyidŏgan*, 1993]). Using a viscoelastic layered earth model [*Yu et al.*, 1999], we calculated a maximum post-seismic deformation from this earthquake at our profile of 2.2 radians. Therefore, we conclude that the observed phase change represents the gradual accumulation of interseismic strain.

Modelling of interseismic strain accumulation

To analyse the variation of phase (or displacement) across the fault, we use a simple model in which right-lateral aseismic slip, s, occurs at depth on a vertical fault beneath a locked upper crust of thickness d. For buried faults, the displacements, y, at distance x from the fault are equivalent to those caused by an infinitely-long screw dislocation in an elastic half-space ($y = \frac{s}{\pi} \tan^{-1} \frac{x}{d}$) [*Savage and Burford*, 1973]. The model assumes pure right-lateral slip on a vertical fault. Failure to meet these conditions would produce an asymmetrical deformation pattern, which is not evident. Additional data from ascending satellite passes would enable this to be tested, but few data are available for ascending passes in this location.

The slip rate on the fault and the elastic lid thickness were determined by minimising the misfit between the model displacements, converted to phase changes, and the observed phase profile (Fig. 3a), assuming that slip at depth is coincident with the surface trace of the North Anatolian Fault. The best-fit model has 22 mm/yr of slip beneath a 14 km elastic lid. The fit to this simple model is good up to distances of 100 km away from the fault. Towards the southern end of our profile the model diverges from the observations where the profile crosses the Ovacik Fault. It is tempting to ascribe this to left-lateral slip of ∼5 mm/yr on that fault. However, the sign of the phase change across the Ovacik fault reverses in the eastern half of our interferogram, and we cannot be confident that this small signal is resolvable above the atmospheric noise.

A-posteriori errors on the slip rate and fault locking depth are determined using a Monte-Carlo simulation technique (Fig. 3b). There is a clear trade-off between the fault locking depth and slip rate that arises because of the tight constraint on phase gradient near the fault: larger slip rates require deeper locking depths. Solutions within the 68% confidence ellipse range in slip rate from 17 to 32 mm/year and in locking depth from 5 to 33 km. If we use the GPS-determined slip rate of 24 ± 1 mm/year, the locking depth is constrained to 18 ± 6 km. The GPS slip rate is an upper bound and assumes a constant slip rate for the whole North Anatolian Fault, on a single fault strand. Nevertheless, it provides a good fit to the GPS points in this region.

Discussion

Strain accumulation across the North Anatolian Fault is consistent with slip at depth on a single fault plane. If the accumulated elastic strain across the eastern North Anatolian Fault is eventually released in earthquakes on the locked, shallow part, then no permanent deformation will result either side of the fault. This would explain the lack of palaeomagnetic rotations along the North Anatolian Fault [*Platzman et al.*, 1994], and the apparent plate-like behaviour of Central Anatolia [*Le Pichon et al.*, 1995].

The observed distribution of deformation across the eastern end of the North Anatolian Fault clearly differs from that seen in areas of distributed strike-slip faulting like the Marlborough Fault Zone [*Bourne et al.*, 1998] and Southern California [*Shen et al.*, 1996], which probably results from distributed deformation at depth [*Prescott and Nur*, 1981; *Bourne et al.*, 1998]. However, because the slip at depth is filtered through the elastic upper crust, we cannot distinguish slip on a buried single fault from slip on a buried shear zone narrower than ∼75 km [*Savage*, 1990].

Conditions at the east end of the North Anatolian Fault are optimal for using InSAR to determine interseismic strain accumulation: relatively large rates, reasonable coherence over intervals ∼2 years, and a fault orientation almost perpendicular to the ERS descending ground track. Nonetheless, the fact that interseismic strain can be isolated there suggests that the same can be done elsewhere, even where the rates are lower and viewing geometry poorer, provided a sufficient number of suitable interferograms can be obtained. Our attempts to determine crustal deformation further west on the North Anatolian Fault failed due to the much poorer coherence that results, at the 56 mm, C-band wavelength of ERS, from the heavier vegetation there. In arid and semi-arid regions, however, coherence can be maintained for upwards of 5 years. The method described in this paper should therefore enable interseismic crustal deformation to be determined in such regions using radar interferometry.

Acknowledgments. This work has been supported by the Natural Environment Research Council, ESA, NASA and a NERC research studentship, with Nigel Press Associates, to TJW. We thank Philip England, Mark Haynes, Margaret Moore and 2 anonymous reviewers for helpful comments/discussions; CNES and Kurt Feigl for support with the DIAPASON interferometric software and Paul Rosen and Scott Hensley of JPL for the use of their ROI_pac software to generate our DEM. Figures were prepared using the public domain GMT software [*Wessel and Smith*, 1998].

References

Barka, A., Slip distribution along the North Anatolian Fault associated with the larger earthquakes of the period 1939 to 1967, *Bull. Seismol. Soc. Am.*, *86*, 1,238–1,254, 1996.

Barka, A., and H. Eyidŏgan, The Erzincan earthquake of 13 March 1992 in Eastern Turkey, *Terra Nova*, *5*, 190–194, 1993.

Bourne, S., T. Arnadottir, J. Beavan, D. Darby, P. England, B. Parsons, R. Walcott, and P. Wood, Crustal deformation of the Marlborough fault zone in the South Island of New Zealand: Geodetic constraints over the interval 1982–1994., *J. Geophys. Res.*, *103*, 30,147–30,165, 1998a.

Bourne, S., P. England, and B. Parsons, The motion of crustal blocks driven by flow of the lower lithosphere and implications for slip rates of continental strike-slip faults, *Nature*, *391*, 655–659, 1998b.

Bürgmann, R., P. Rosen, and E. Fielding, Synthetic aperture radar interferometry to measure Earth's surface topography and its deformation, *Ann. Rev. Earth. Planet. Sci.*, *28*, 169–209, 2000a.

Delacourt, C., P. Briole, and J. Achache, Tropospheric corrections of SAR interferograms with strong topography. Application to Etna, *Geophys. Res. Lett.*, *25*, 2,849–2,852, 1998.

Goldstein, R. M., and C. L. Werner, Radar interferogram filtering for geophysical applications, *Geophys. Res. Lett.*, *25*, 4,035–4,038, 1998.

Le Pichon, X., N. Chamot-Rooke, S. Lallemant, R. Noomen, and G. Veis, Geodetic determination of the kinematics of central Greece with respect to Europe: Implications for eastern Mediterranean tectonics, *J. Geophys. Res.*, *100*, 12,765–12,690, 1995.

Massonnet, D., and K. L. Feigl, Radar interferometry and its application to changes in the earth's surface, *Rev. Geophys.*, *36(4)*, 441–500, 1998.

Massonnet, D., M. Rossi, C. Carmona, F. Adragna, G. Peltzer, K. Fiegl, and T. Rabaute, The displacement field of the Landers earthquake mapped by radar interferometry, *Nature*, *364*, 138–142, 1993.

McClusky, S., et al., Global Positioning System constraints on plate kinematics and dynamics in the eastern Mediterranean and Caucasus, *J. Geophys. Res.*, *105*, 5,695–5,719, 2000.

Platzman, E., J. Platt, C. Tapirdamaz, M. Sanver, and C. Rundle, Why are there no clockwise rotations along the North Anatolian Fault Zone, *J. Geophys. Res.*, *99*, 21,705–21,715, 1994.

Prescott, W., and A. Nur, The accommodation of relative motion at depth on the San Andreas fault system in California, *J. Geophys. Res.*, *86*, 999–1,004, 1981.

Rosen, P., C. Werner, E. Fielding, S. Hensley, S. Buckley, and P. Vincent, Aseismic creep along the San Andreas Fault northwest of Parkfield, CA measured by radar interferometry, *J. Geophys. Res.*, *25*, 825–828, 1998.

Şaroglu, F., Ö. Emre, and İ. Kuşçu, *Active Fault Map of Turkey*, General Directorate of Mineral Research and Exploration (MTA), Eskişehir Yolu, 06520, Ankara, Turkey, 1992.

Savage, J., Equivalent strike-slip earthquake cycles in half space and lithospheric-asthenosphere earth models, *J. Geophys. Res.*, *95*, 4,873–4,879, 1990.

Savage, J., and R. Burford, Geodetic determination of relative plate motion in Central California., *J. Geophys. Res.*, *78*, 832–845, 1973.

Scharroo, R., and P. Visser, Precise orbit determination and gravity field improvement for the ERS satellites, *J. Geophys. Res.*, *103*, 8,113–8,127, 1998.

Scholz, C., *The Mechanics of Earthquakes and Faulting*, Cambridge University Press, Cambridge, 1990.

Shen, Z.-k., L. y. Sung, D. Dong, B. King, and S. McClusky, Crustal Deformation Working Group of the Southern California Earthquake Center, Horizontal crustal deformation velocity map, version 1.0, 1996, *http://minotaur.ess.ucla.edu/velmap/welcome.shtml*.

Wessel, P., and W. H. F. Smith, New, improved version of generic mapping tools released, *Eos Trans. AGU*, *79*, 579, 1998.

Yu, T., J. Rundle, and J. Fernández, Correction to "Surface deformation due to a strike-slip fault in an elastic gravitational layer overlying a viscoelastic gravitational half-space" by Ting-To Yu, John B. Rundle and José Fernández, *J. Geophys. Res.*, *104*, 15,313–15,315, 1999.

Zebker, H., P. Rosen, and S. Hensley, Atmospheric effects in interferometric synthetic aperture radar surface deformation and topographic maps, *J. Geophys. Res.*, *102*, 7,547–7,563, 1997.

Barry Parsons, Tim Wright, Department of Earth Sciences, University of Oxford, Parks Road, Oxford, UK. (e-mail: barry@earth.ox.ac.uk;timw@earth.ox.ac.uk)

Eric Fielding, JetPropulsion Laboratory, 4800 Oak Grove Drive,Pasadena, CA, 91109, USA. (e-mail: ericf@sierras.jpl.nasa.gov)

(Received January 10, 2001; accepted February 7, 2001.)